arXiv:2506.05786v1 [cond-mat.mes-hall] 6 Jun 2025

Robust quantification of the diamond nitrogen-vacancy center charge state via photoluminescence spectroscopy

G. Thalassinos,[1, a)] D. J. McCloskey,[2, 3] A. Mameli,[1] A. J. Healey,[1] C. Pattinson,[2, 3] D. Simpson,[2, 3] B. C. Gibson,[1] A. Stacey,[1] N. Dontschuk,[2, b)] and P. Reineck[1, c)]

[1)] *School of Science, RMIT University, Melbourne, VIC 3001, Australia*

[2)] *School of Physics, University of Melbourne, Parkville, VIC 3010, Australia*

[3)] *Australian Research Council Centre of Excellence in Quantum Biotechnology, School of Physics, University of Melbourne, Parkville, VIC 3010, Australia*

Nitrogen vacancy (NV) centers in diamond are at the heart of many emerging quantum technologies, all of which require control over the NV charge state. Hence, methods for quantification of the relative photoluminescence (PL) intensities of the NV^0 and NV^- charge state, i.e., a charge state ratio, are vital. Several approaches to quantify NV charge state ratios have been reported but are either limited to bulk-like NV diamond samples or yield qualitative results. We propose an NV charge state quantification protocol based on the determination of sample- and experimental setup-specific NV^0 and NV^- reference spectra. The approach employs blue (400–470 nm) and green (480–570 nm) excitation to infer pure NV^0 and NV^- spectra, which are then used to quantify NV charge state ratios in subsequent experiments via least squares fitting. We test our dual excitation protocol (DEP) for a bulk diamond NV sample, 20 and 100 nm nanodiamond particles and compare results with those obtained via other commonly used techniques such as zero-phonon line fitting and non-negative matrix factorization. We find that DEP can be employed across different samples and experimental setups and yields consistent and quantitative results for NV charge state ratios that are in agreement with our understanding of NV photophysics. By providing robust NV charge state quantification across sample types and measurement platforms, DEP will support the development of NV-based quantum technologies.

I. INTRODUCTION

The nitrogen vacancy (NV) center in diamond is one of the most widely adopted platforms for emerging quantum technologies[1–3]. In bulk diamond, NV centers are generally present in either a neutral (NV^0) or a negative charge state (NV^-). Although both charge states are photoluminescent, only NV^- has an optically addressable spin that allows for spin-based optical quantum sensing, enabling applications including magnetometry[4] and thermometry[5]. Furthermore, the NV charge state itself can be used as an all-optical nanoscale voltage[6] and electric-field sensor[7]. Hence, significant materials engineering[8] and photonics[9,10] efforts are underway to control and tailor the NV charge state for specific applications.

Underpinning all of these efforts is the ability to quantify the NV charge state. While the two charge states can be clearly identified in PL spectra via their zero-phonon lines (ZPLs) at 575.07 nm (2.156 eV, NV^0) and 637.45 nm (1.945 eV, NV^-), their phonon side-bands (PSBs) overlap significantly (fig. 1A)[11–13], making precise quantification of the relative contribution of each charge state to the overall NV PL non-trivial. Several approaches for the quantification of the NV charge state have been reported. One approach uses the intensity ratio of the two ZPLs as a measure of the relative contribution of each charge state to the overall PL signal[14–17]. This approach is feasible for NV ensemble measurements in bulk diamond samples, where pronounced NV ZPLs are generally observed, particularly at low temperatures[18]. However, for NV centers in small nanodiamonds[11,19,20] and, more generally, for NV centers within a few nanometers of the diamond surface[6], ZPLs are weak or not visible at all in PL spectra. Thus, another approach to quantify the NV charge state ratio is based on the use of 'pure' NV^0 and NV^- spectra from literature such as reference[11] that are used as fits in other laboratories[21–23]. However, NV spectral profiles can vary depending on the diamond properties (e.g., strain), sample dimensions (bulk vs. nanoparticles), environmental factors like temperature[24,25], the nanoscale environment[26], and the spectroscopy equipment used. As a result, the seemingly simple question 'How far into the far-red do NV^0 and NV^- emit?' has no simple answer based on the current literature (see SI Table S1). Hence, pure NV^0 and NV^- spectra are ideally acquired in a sample- and equipment-specific manner.

To this end, three main approaches have been reported. The first two approaches are photoluminescence (PL) decomposition analysis[15] and a similar microwave-assisted decomposition technique[25]. The former modulates the NV charge state via the excitation power to change the NV^- ionization rate; the latter modulates the NV^- PL intensity using microwaves. Both techniques use their respective modulation to first derive the spectral profile of NV^-. Then, this NV^- reference is subtracted from a mixed NV^0/NV^- signal until there is no visible ZPL peak at 637 nm to determine NV^0. The third approach employs machine learning which does not require *a-priori* knowledge about the NV ZPLs in order to derive a set

[a)] Electronic mail: giannis.thalassinos@rmit.edu.au
[b)] Electronic mail: dontschuk.n@unimelb.edu.au
[c)] Electronic mail: philipp.reineck@rmit.edu.au

of pure NV spectra. Non-negative matrix factorization (NNMF) is an often used algorithm for decomposition of spectra into an integer number of non-negative components for a given set of training data. The training set consists of a series of NV spectra, where each spectrum contains different relative contributions of NV^0 and NV^-[27–30]. However, it is not clear that NNMF accurately determines the "true" NV^0/NV^- spectral profiles. Compared to experiment[11–13,15,18,22,25,31–33], NNMF predicts that the maximum emission wavelength of NV^0 is significantly shorter than NV^- by >70 nm (see SI Table S1)[27–30] and can show the presence of the NV^- ZPL in the 'pure' NV^0 spectrum and/or vice-versa[29]. Therefore, new approaches are needed.

Here, we propose a dual wavelength excitation protocol (DEP) for measuring the pure NV^0 and NV^- spectral profiles, which are used to determine the NV charge state ratio. We show that this method works across a wide variety of diamond types, including bulk diamond and nanoparticles; and vastly different optical configurations, including confocal microscopes and nanoparticles in suspension. We leverage the direct photo-ionization of NV^- using blue/violet excitation (<470 nm) to obtain a pure NV^0 spectrum, which is then used to determine the NV^- spectrum. NV^0 and NV^- reference spectra are then fit to experimental data using the linear least-squares fitting algorithm to determine the NV charge state ratio. We benchmark this technique against ZPL fitting, NNMF, and skewed Gaussian (SG) fitting to approximate the 'pure' NV spectra. We demonstrate that our protocol works across a range of samples and measurement techniques, even in the absence of ZPLs. Our protocol enables robust quantification of the NV charge state and will thereby aid the development of next-generation quantum sensing materials and protocols.

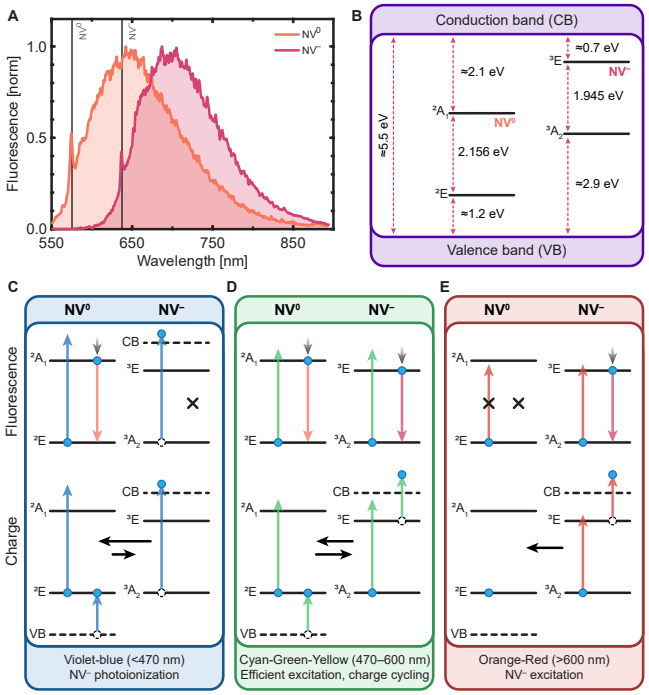


FIG. 1. NV center photodynamics. **A:** Fluorescence spectra of NV^0 and NV^- with characteristic ZPLs at 575 and 637 nm (marked via vertical lines), respectively, showing significant overlap between 600–850 nm. **B:** Energy level diagram of NV^0 and NV^- within the diamond band gap. **C-E:** Dynamics of the NV center under different excitation wavelengths. Violet-blue excitation (C) leads to single-photon photoionization of NV^- into NV^0, while still exciting NV^0, which relaxes down to the ground state via fluorescence. Green illumination (D) leads to efficient excitation of both charge states and allows for dynamic charge state switching via ionization and re-pumping processes. Red light (E) has insufficient energy to promote NV^0 to the excited state, leading exclusively to NV^- emission. Horizontal, black lines indicate charge state switching, with relative length indicative of the rate in a particular direction. Vertical, short grey lines represent phonon relaxations.

II. METHODS

A. Confocal fluorescence spectroscopy

We investigated a commercially available bulk diamond sample (DNV-B14, Element Six) and fluorescent nanodiamonds (FNDs) with a nominal diameter of 100 nm (Adàmas Nanotechnologies) spin-coated onto a Si substrate using our custom-built scanning confocal microscope (SI fig. S1A). Samples were excited using an 80 MHz pulsed laser (Fianium WhiteLase 400-SC, NKT Photonics) operating between 400–700 nm through a 100× objective (NA = 0.9). Fluorescence was collected through the same objective and fibre coupled to an avalanche photodiode (APD) (25 %, SPCM-AQRH-14-TR, Excelitas) and a spectrometer (75 %, SpectraPro SP-2500, Princeton Instruments) with a charge-coupled device (CCD) camera (PIXIS 100BR, Princeton Instruments).

B. In-solution fluorescence spectroscopy

Fluorescent nanodiamonds (FNDs) with nominal sizes of 20 and 140 nm (Adámas Nanotechnologies) were suspended in de-ionized (DI) water at approximately 1.00 and 0.01 mg mL^{-1}, respectively before being measured in our custom-built in-solution spectroscopy setup (SI fig. S1B). Samples were excited using the same pulsed laser as the confocal setup and weakly focused onto the sample cuvette (18FL, FireFlySci). Fluorescence was collected via a custom fibre (105 µm core, NA = 0.22) through an in-line filter mount (FOFMS, Thorlabs) and coupled into the spectrometer. For each excitation wavelength, a water Raman spectrum and a scattering reference using 40 nm SiO_2 nanoparticles were acquired and subtracted from the FND signals (see SI for details).

III. DUAL EXCITATION PROTOCOL

Generally, accurately determining the spectral profile of NV^- can be achieved using any technique which requires at least two measured spectra with a different NV charge state ratio[15,25,27,28,30]. The fundamental challenge lies in the robust determination of the NV^0 spectral profile in the spectral region above 700 nm, where it significantly overlaps with NV^-.

The NV^- ground state is located ≈2.6 eV below the conduction band[13] (fig. 1B). It is efficiently photoionized to NV^0 via a single-photon processes using excitation wavelengths below ≈470 nm, leading to NV^0 emission. In practice, it has been observed that NV PL spectra acquired using excitation wavelengths of 458 nm[12,34] still show some NV^- PL in bulk diamond, which disappears for excitation wavelengths <450 nm. Under green excitation (510–540 nm), both NV charge states are efficiently excited and cycle between each other through ionization and recombination processes (fig. 1D)[13]. Under red excitation (600–640 nm), photons only have sufficient energy to excite NV^- (fig. 1E). Simply, there exist excitation windows in which either one of the two NV charge states is directly excited, or both are. Therefore, by tuning the excitation wavelength, sample-specific reference NV^0/NV^- spectra can be obtained.

Figure 2 illustrates the main steps of our protocol based on measurements performed on commercially available fluorescent nanodiamonds (FNDs) with a nominal size of 140 nm suspended in DI water. Pure NV^0 and mixed NV^0/NV^- fluorescence spectra were acquired using violet (400 nm) and green (520 nm) excitation, respectively, as shown in fig. 2A. The measured spectra are labelled $S_\gamma(\lambda)$ where γ and λ represent the excitation and emission wavelengths, respectively.

Each measured NV signal can be expressed as a linear combination of the two charge states

$$S_\gamma(\lambda) = \alpha(\gamma)\mathrm{NV}^0 + \beta(\gamma)\mathrm{NV}^-, \tag{1}$$

where $\alpha(\gamma)$ and $\beta(\gamma)$ are unknown non-negative scalar quantities representing the relative contribution of each charge state as a function of the excitation wavelength. In the case where γ <470 nm, $\alpha > 0$ and we assume $\beta \approx 0$, yielding us a reference NV^0 spectrum ($NV^0{}_{\mathrm{ref}}$),

$$S_{<470}(\lambda) = \alpha(<470)\mathrm{NV}^0 = \mathrm{NV}^0_{\mathrm{ref}}. \tag{2}$$

NV^- exhibits negligible fluorescence below 600 nm[12], thus both spectra were normalized (denoted by superscript n) between λ = 550–600 nm (highlighted in grey in fig. 2A), via the expression

$$S^n_\gamma(\lambda) = \frac{S_\gamma(\lambda)}{\int_{550}^{600} S_\gamma(\lambda)\, d\lambda}, \tag{3}$$

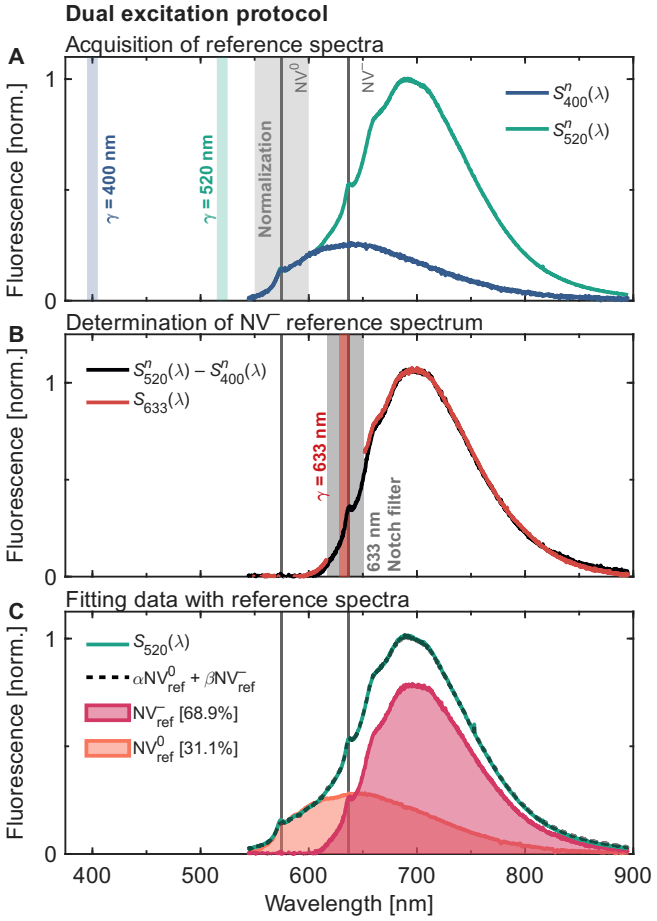


FIG. 2. Dual excitation protocol on 140 nm FNDs suspended in water. **A:** Reference spectra are acquired using 400 and 520 nm excitation to obtain a pure NV^0 signal ($S^n_{400}(\lambda)$) and a mixed NV^0/NV^- spectrum ($S^n_{520}(\lambda)$), respectively, which are then normalized for the same NV^0 contribution between 550–600 nm (shaded region). **B:** A pure NV^- spectrum is obtained by taking the difference between the two reference spectra in (A), which is then compared to experiment under 633 nm illumination ($S_{633}(\lambda)$). **C:** The reference NV^0 and NV^- spectra can then be used to fit experimental data using eq. (1) to determine the charge state ratio.

thus, both signals are normalized to the same NV^0 intensity, or

$$\frac{\alpha(<470)}{\alpha(520)} = 1. \tag{4}$$

This normalization allows us to fully subtract the NV^0 signal from any mixed NV^0/NV^- spectrum, resulting in a pure NV^- reference spectrum ($NV^-{}_{\mathrm{ref}}$), via the relation

$$\mathrm{NV}^-_{\mathrm{ref}} = S^n_{470-600}(\lambda) - S^n_{<470}(\lambda), \tag{5}$$

as seen in fig. 2B. Here, we see that the NV^- ZPL correctly appears at 637 nm, with no sign of NV^0 fluorescence. For verification, we investigated the same sample

under 633 nm (1.959 eV) excitation, which only has sufficient energy to excite NV^-, labeled ($S_{633}(\lambda)$). We found that red excitation leads to no detectable NV^0 signal and is nearly identical to the DEP derived NV^- spectrum.

With these two measurements, we can fit any combination of NV^0 and NV^- using the least squares method to determine the relative contribution of each charge state and precisely determine the NV^- contribution via the expression

$$NV^- = \frac{\beta(\gamma) \int_{\lambda=0}^{\inf} NV^-_{ref}(\lambda)\, d\lambda}{\int_{\lambda=0}^{\inf} \alpha(\gamma) NV^0_{ref}(\lambda) + \beta(\gamma) NV^-_{ref}(\lambda)\, d\lambda}. \quad (6)$$

An example is provided in fig. 2C, where the two reference spectra are used to fit the original green data ($S_{520}(\lambda)$), revealing an NV^- contribution of 68.9 %.

A. Benchmarking

We tested our protocol for three different samples across two measurement techniques. First, we investigated a commercially available bulk diamond sample with clear NV ZPLs under a confocal microscope, representing the simple case. Second, we suspended an ensemble of 20 nm FNDs in DI water and analyzed them using our in-solution setup. Finally, we analyzed 100 nm FND particles under a confocal microscope. For each test cases, we compared our protocol against three other methods for determining the charge state ratio: ZPL fitting, fitting a skewed Gaussian (SG) model, and NNMF (see SI for details).

We excited the bulk sample using a tunable laser from 405–520 nm (bandwidth of 10 nm) at a constant power of 5 µW using a custom-built confocal microscope. Normalized fluorescence spectra acquired using different excitation wavelengths are shown in fig. 3A. The spectra show mostly NV^0 PL for excitation wavelengths 405–470 nm. For longer wavelengths, the NV^- contribution continuously increases up to the highest investigated excitation wavelength of 520 nm. The spectra were then analyzed using the different methods mentioned above to determine the NV^- ratio as a function of excitation wavelength (fig. 3B, for fitting of individual spectra using each technique, see SI fig. S2-S5). All protocols yield a constant NV ratio below 470 nm excitation, which then increases with excitation wavelength up to 520 nm excitation. DEP, NNMF, and SG fitting were all capable of fitting each combination of NV^0 and NV^- with a R^2 of > 0.98, with NNMF being the highest on average (SI fig. S6). Both DEP and ZPL fitting yield an NV^- ratio of 0 % below 470 nm excitation, which increases to 60 % as the excitation wavelength increases to 520 nm. SG and NNMF on the other hand yield a significantly higher minimum NV^- contribution of 10 % and 40 %, respectively, below 470 nm excitation, which increases to 70 % and 80 % for 520 nm excitation.

Assuming that excitation below 450 nm should result in pure NV^0 fluorescence[12,13,35], the presence of NV^- in these fits is indicative of an underestimate of how far into the red spectral region the NV^0 emission extends. Indeed, the NNMF output for the pure NV^0 spectrum (SI fig. S7), suggests that NV^0 does not emit above 750 nm, while our measurements using 400 nm excitation suggest that NV^0 emission extends well above 800 nm. Overall, the data in fig. 3A and B show that both DEP and ZPL fitting yield very similar results in this case, both of which are in agreement with our current understanding of NV charge state photophysics. Both NNMF and SG methods, even in this relatively simple case, overestimate the NV^- contribution to the NV PL spectra.

As a second, more challenging test case, we investigated an ensemble of commercially available 20 nm FNDs suspended in water. FNDs of this size typically show predominantly NV^0 PL and the ZPLs of both charge states are weak and, in some cases, not visible at all[19,28]. Figure 3C shows normalized PL spectra of the 20 nm FNDs in suspension as a function of 520 nm laser excitation power in the range from 0.6 to 22 mW. The PL spectra slightly red-shift with increasing excitation power, which suggests an increase in the NV^- contribution with increasing excitation power caused by increased photocycling rates.

We again used the four different analysis approaches to quantify the above observations, with results shown in fig. 3D. DEP yields a monotonic increase in the NV^- ratio from 17 % to 27 % with increasing excitation power. While SG and NNMF yield a comparable relative increase in the NV^- contribution with increasing excitation power, both appear to overestimate the absolute NV^- ratio by up to 24 %. ZPL fitting yields inconsistent results, though these are typically bounded by the values obtained from the other analysis techniques. ZPL fitting is inconsistent mainly because peak fitting becomes extremely sensitive to minor changes in both signal and noise for weak ZPLs such as those observed in 20 nm FNDs. Given the relative importance of near-surface NV centers in bulk diamond and FNDs in current research, the ability of DEP to quantify small changes in the NV^- ratio even in the absence of strong ZPLs is a major strength of our technique.

Lastly, we tested our approach for 100 nm FNDs dispersed on a silicon wafer substrate, imaged with a scanning confocal fluorescence microscope connected to a spectrometer. We collected PL spectra for 27 FNDs (or small FND aggregates) using 405 and 520 nm excitation (the fluorescence map with marked FNDs can be found in SI fig. S8). We averaged all spectra acquired using 405 nm excitation to be used as the NV^0 reference for DEP. The PL spectrum for each particle was normalized and ordered by increasing NV^- PL intensity, quantified as the integrated fluorescence above 650 nm divided by the integrated fluorescence below 650 nm, shown in fig. 3E. Here, we see significant variability in the NV charge state ratio between individual particles,

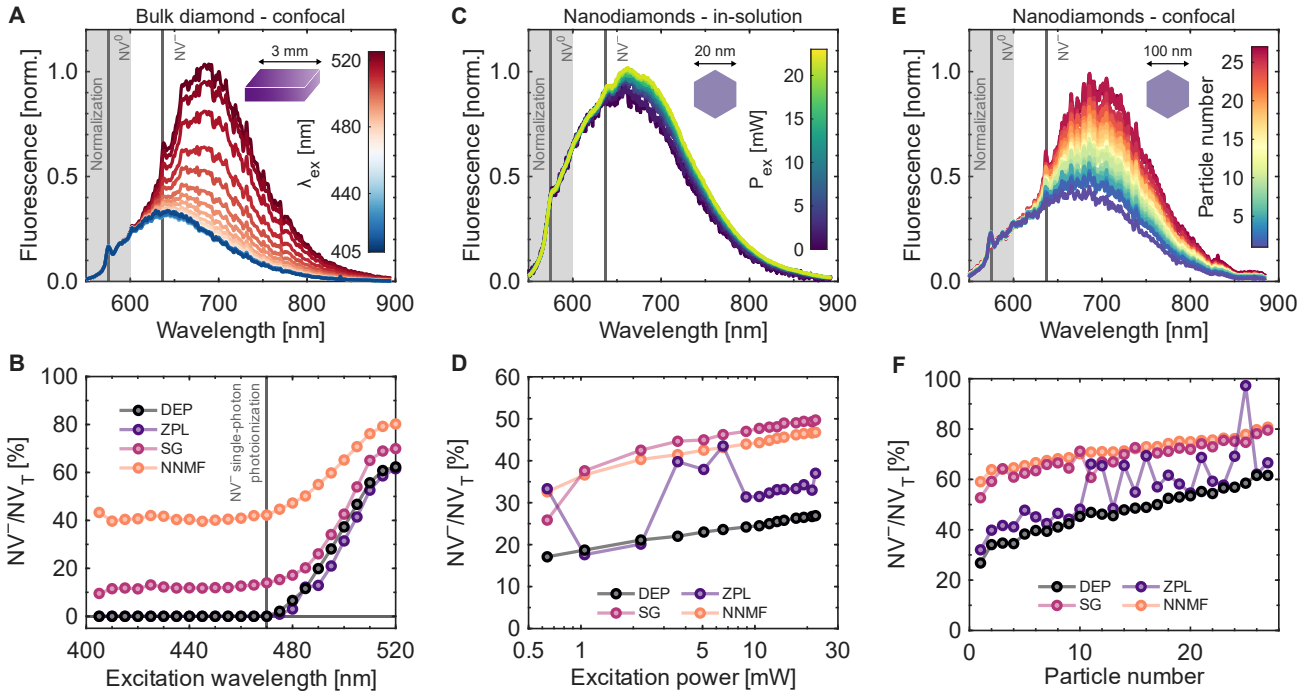


FIG. 3. NV charge state ratio protocol comparison. **A:** Fluorescence spectra of bulk diamond for excitation wavelengths (λ_{ex}) ranging 405–520 nm under a confocal microscope. **B:** NV^- contribution of the bulk diamond using our dual-excitation protocol (DEP), ZPL, Skewed Gaussian (SG), and NNMF fitting. The vertical line roughly indicates the wavelength we expect to see single-photon photoionization of NV^-. **C:** Fluorescence spectra of 20 nm FNDs suspended in DI water, excited using 520 nm for excitation powers (P_{ex}) between 0.64–22.30 mW. **D:** NV^- contribution of the 20 nm FNDs as a function of excitation power. **E:** Fluorescence spectra of dispersed 100 nm FNDs under a confocal microscope, ordered by increasing NV^- content. **F:** NV^- contribution for all 100 nm particles using each protocol. All spectra (A, C, E) were normalized between 550–600 nm (shaded regions), with vertical lines marking the positions of the NV ZPLs.

with some consisting almost entirely of NV^0 while others show predominately NV^-, consistent with prior reports[27]. Figure 3F shows the NV^- ratio determined by all four analysis approaches for all particles. As observed in the previous two test cases, both SG and NNMF yield a higher NV^- contribution, ranging from ≈55–80 %, compared to both ZPL and DEP (fig. 3F). DEP suggests the NV^- contribution ranges from 27–62 % with an average of 47 ± 9 %. For many particles, ZPL fitting and DEP yield very similar results. However, since the ZPL lines are very pronounced for some particles and are barely visible for others, the NV^- ratios determined using the ZPL fitting approach are quite susceptible to artefacts and, consequently, exhibit far greater variation. We do not, therefore, attribute the observed variation to intrinsic properties of the analysed particles.

B. Workflow

We propose a simple workflow for the implementation of our protocol, which is summarized in fig. 4. Only two primary measurements (fig. 4, top row) are required for the determination of pure NV^- and NV^0 reference spectra; one PL spectrum acquired using green (480-570 nm) excitation that contains contributions from both charge states, and one PL spectrum acquired using blue (<470 nm) excitation for a pure NV^0 spectrum. Next, all background signals must be acquired and removed from the two reference spectra. Background signals are system and sample dependent, but in many cases this step may only require a simple background subtraction due to detector dark counts. In some cases however, background signals may be more complex, such as Raman signals from the diamond host or the surrounding media (e.g., water) in the case of FND suspensions.

Generally, the acquisition and subtraction of these background spectra is very effective, and we present a complex example of such background removal in SI fig. S9. Once all background signals are accounted for, the two spectra (NV^0+NV^- and NV^0 only) are normalized between 550–600 nm to the same NV^0 contribution. Then, the NV^0 spectrum is subtracted from the spectrum containing both charge states to yield a pure NV^- reference spectrum. Finally, the two reference spectra can be fit to data of interest using a least squares fitting routine to determine the relative contribution of each NV charge state to the overall fluorescence signal.

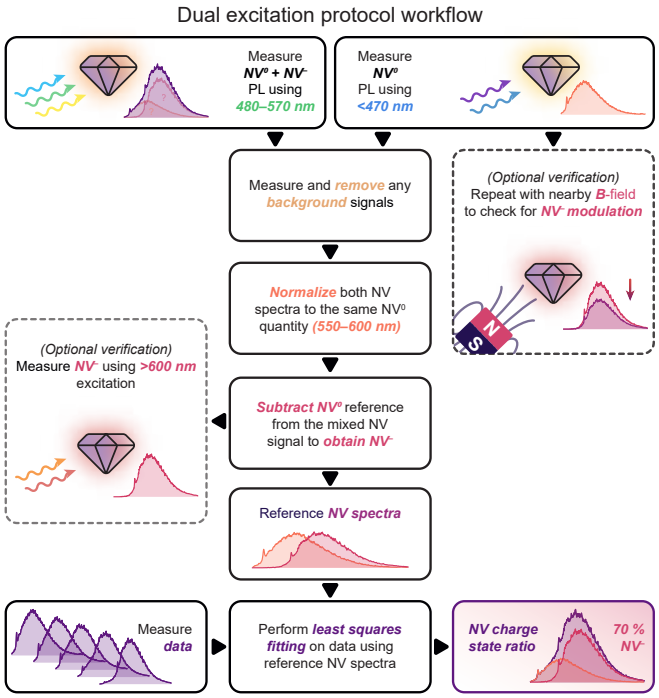


FIG. 4. Dual excitation protocol workflow. DEP requires two initial measurements taken with < 470 nm and 480–570 nm to obtain reference NV^0 and mixed NV^0/NV^- spectra. Background signals must be removed from the two measurements before normalization between 550–600 nm. Once normalized, the difference between the signals can be calculated to obtain the NV^- reference spectrum. Once both reference spectra are determined, they can be used to fit data to determine the relative contribution of each charge state.

C. Verification and refinement

Two optional steps can be introduced to verify the NV reference spectra. Firstly, it is possible under certain conditions to observe NV^- PL using photon energies above 2.63 eV (below 470 nm) which would normally photoionize NV^- and create NV^0. Therefore, an additional step may be introduced to check for NV^- modulation under $<$470 nm excitation in an external magnetic field, which is known to affect the NV^- quantum yield[36,37], but not NV^0. Secondly, an excitation wavelength of $>$600 nm can be used to generate a pure NV^- spectrum. Generally, optical notch filters would be required to remove the excitation light signal from the PL spectrum, blocking part of the NV spectrum. Nevertheless, the resulting NV spectrum can be used to optimize the normalization window before the NV^0 reference is subtracted from the mixed NV^0/NV^- signal, or used to remove any remaining NV^- in the NV^0 reference.

Here, we measure the NV fluorescence of a bulk diamond sample under both blue (430 nm) and red (630 nm) excitation wavelengths (fig. 5A and B, respectively) with and without the presence of an external magnetic field applied via permanent magnet. Under blue excitation,

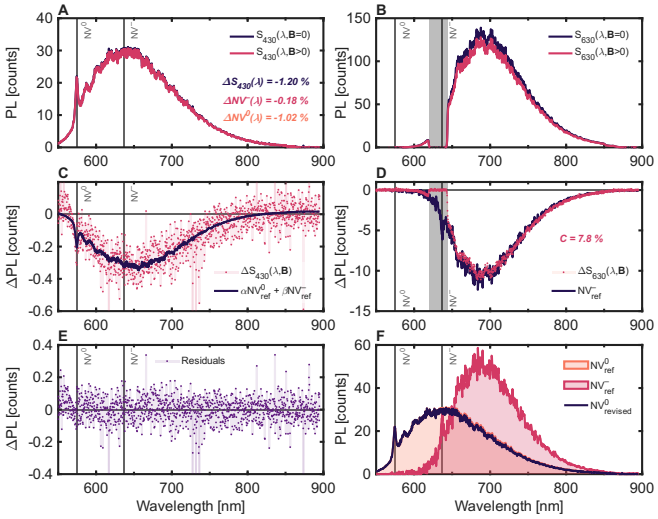


FIG. 5. NV fluorescence spectra measured using an excitation wavelength of 430 nm (A) and 630 nm (B) with and without the presence of an external $\vec{B}$-field, with the difference shown in (C) and (D), respectively. The change in fluorescence under 430 nm is fit with the NV reference spectra, with residuals shown in (E). F: original and revised NV reference spectra.

fig. 5C shows a 1.20 % reduction in overall fluorescence when the magnet is introduced. Fitting the NV reference spectra using eq. (1) allows us to approximate the change in fluorescence attributable to NV^-, which we find to be on order 0.18 % (residuals in fig. 5E). We show that NV^- is reduced by 7.8 % under the same applied $\vec{B}$-field, which we determine through red (630 nm) excitation and display in fig. 5D. Under this excitation condition, the change in fluorescence can be attributed solely to spin mixing induced by the magnetic field. Assuming that the total NV^- is also modulated to the same degree under 430 nm excitation, we can determine how much NV^- exists under 430 nm excitation via

$$\beta_0 = \frac{\Delta\beta}{C} \tag{7}$$

where β_0 is the NV^- scaling factor under no magnetic field, $\Delta\beta$ is the change in the NV^- scaling factor after the magnet is introduced, and C is the contrast observed under 630 nm (see fig. 5D). By approximating β_0, we can subtract any remaining NV^- from the NV^0 reference via

$$\mathrm{NV}^0_{\mathrm{revised}} = \mathrm{NV}^0_{\mathrm{ref}} - \beta_0 \mathrm{NV}^-, \tag{8}$$

to obtain a revised NV^0 reference spectrum which is $\approx$ 2 % different to our original approximation as shown in fig. 5F. We note that this correction is still an approximation, as the the fit used to determine $\Delta\beta$ uses an NV^0 reference which may contain some small fraction of NV^- and thus lead to a slight underestimate of $\Delta\beta$. Nevertheless, the change is relatively small, which increases our

confidence that blue excitation is sufficient for NV charge state determination.

IV. CONCLUSION

We investigated several approaches for calculating the NV^0/NV^- charge state ratio, particularly for diamond samples which do not exhibit pronounced zero-phonon lines (ZPLs), such as nanodiamonds. We tested ZPL fitting, two algorithmic approaches, namely fitting a skewed Gaussian model of the NV^0/NV^- spectral profiles and non-negative matrix factorization, and our dual excitation protocol (DEP), which employs blue (400–470 nm) and green (480–570 nm) excitation to derive a set of sample- and setup-specific pure NV^0/NV^- spectra to fit subsequent experiments. We evaluated each approach for a variety of different samples and optical systems, including bulk diamond and dispersed 100 nm nanodiamonds under a scanning confocal microscope, and 20 nm nanodiamonds in aqueous suspension. We demonstrate that DEP is capable of deriving quantitative NV charge state ratios that are consistent with our understanding of NV photophysics across common sample types and measurement setups.

ACKNOWLEDGEMENTS

We acknowledge the support of the Australian Research Council (ARC) through a Discovery Project (DP220102518) and the ARC Centre of Excellence in Quantum Biotechnology (CE230100021). GT acknowledges support through an ARC Linkage grant (LP210300230) in collaboration with Diamond Defence Pty Ltd. DJM acknowledges support through a University of Melbourne McKenzie Fellowship. ND acknowledges support through a Department of Defense NSDIRG grant (NS220100071). PR acknowledges support through an ARC DECRA Fellowship (DE200100279) and an RMIT University Vice-Chancellor's Senior Research Fellowship. This work was carried out in part at RMIT University's Microscopy & Microanalysis Facility, a linked laboratory of Microscopy Australia enabled by the National Collaborative Research Infrastructure Strategy (NCRIS).

CONFLICT OF INTEREST STATEMENT

The authors have no conflicts to disclose.

DATA AVAILABILITY STATEMENT

Data available on request from the authors.

REFERENCES

[1] R. Schirhagl, K. Chang, M. Loretz, and C. L. Degen, "Nitrogen-vacancy centers in diamond: Nanoscale sensors for physics and biology," Annual review of physical chemistry **65**, 83–105 (2014).
[2] S. Pezzagna and J. Meijer, "Quantum computer based on color centers in diamond," Applied Physics Reviews **8**, 011308 (2021).
[3] J. Wrachtrup and F. Jelezko, "Processing quantum information in diamond," J. Phys.: Condens. Matter **18**, S807 (2006).
[4] L. Rondin, J.-P. Tetienne, T. Hingant, J.-F. Roch, P. Maletinsky, and V. Jacques, "Magnetometry with nitrogen-vacancy defects in diamond," Rep. Prog. Phys. **77**, 056503 (2014).
[5] P. Neumann, I. Jakobi, F. Dolde, C. Burk, R. Reuter, G. Waldherr, J. Honert, T. Wolf, A. Brunner, J. H. Shim, D. Suter, H. Sumiya, J. Isoya, and J. Wrachtrup, "High-Precision Nanoscale Temperature Sensing Using Single Defects in Diamond," Nano Lett. **13**, 2738–2742 (2013).
[6] D. J. McCloskey, N. Dontschuk, A. Stacey, C. Pattinson, A. Nadarajah, L. T. Hall, L. C. L. Hollenberg, S. Prawer, and D. A. Simpson, "A diamond voltage imaging microscope," Nat. Photon. **16**, 730–736 (2022).
[7] F. Dolde, H. Fedder, M. W. Doherty, T. Nöbauer, F. Rempp, G. Balasubramanian, T. Wolf, F. Reinhard, L. C. L. Hollenberg, F. Jelezko, and J. Wrachtrup, "Electric-field sensing using single diamond spins," Nature Phys **7**, 459–463 (2011).
[8] Y. Doi, T. Fukui, H. Kato, T. Makino, S. Yamasaki, T. Tashima, H. Morishita, S. Miwa, F. Jelezko, Y. Suzuki, and N. Mizuochi, "Pure negatively charged state of the NV center in n-type diamond," Phys. Rev. B **93**, 081203 (2016).
[9] A. A. Wood, A. Lozovoi, R. M. Goldblatt, C. A. Meriles, and A. M. Martin, "Wavelength dependence of nitrogen vacancy center charge cycling," Phys. Rev. B **109**, 134106 (2024).
[10] J. F. Barry, J. M. Schloss, E. Bauch, M. J. Turner, C. A. Hart, L. M. Pham, and R. L. Walsworth, "Sensitivity optimization for NV-diamond magnetometry," Rev. Mod. Phys. **92**, 015004 (2020).
[11] L. Rondin, G. Dantelle, A. Slablab, F. Grosshans, F. Treussart, P. Bergonzo, S. Perruchas, T. Gacoin, M. Chaigneau, H.-C. Chang, V. Jacques, and J.-F. Roch, "Surface-induced charge state conversion of nitrogen-vacancy defects in nanodiamonds," Phys. Rev. B **82**, 115449 (2010).
[12] N. B. Manson, M. Hedges, M. S. J. Barson, R. Ahlefeldt, M. W. Doherty, H. Abe, T. Ohshima, and M. J. Sellars, "NV^-–N^+ Pair Centre in 1b Diamond," New J. Phys. **20**, 113037 (2018).
[13] N. Aslam, G. Waldherr, P. Neumann, F. Jelezko, and J. Wrachtrup, "Photo-induced ionization dynamics of the nitrogen vacancy defect in diamond investigated by single-shot charge state detection," New J. Phys. **15**, 013064 (2013).
[14] VM. Acosta, E. Bauch, MP. Ledbetter, C. Santori, K.-M. Fu, PE. Barclay, RG. Beausoleil, H. Linget, JF. Roch, F. Treussart, S. Chemerisov, W. Gawlik, and D. Budker, "Diamonds with a high density of nitrogen-vacancy centers for magnetometry applications," Physical Review B **80**, 115202 (2009).
[15] S. T. Alsid, J. F. Barry, L. M. Pham, J. M. Schloss, M. F. O'Keeffe, P. Cappellaro, and D. A. Braje, "Photoluminescence Decomposition Analysis: A Technique to Characterize N-V Creation in Diamond," Phys. Rev. Applied **12**, 044003 (2019).
[16] K.-M. C. Fu, C. Santori, P. E. Barclay, and R. G. Beausoleil, "Conversion of neutral nitrogen-vacancy centers to negatively charged nitrogen-vacancy centers through selective oxidation," Appl. Phys. Lett. **96**, 121907 (2010).
[17] C. Shinei, M. Miyakawa, S. Ishii, S. Saiki, S. Onoda, T. Taniguchi, T. Ohshima, and T. Teraji, "Equilibrium charge state of NV centers in diamond," Appl. Phys. Lett. **119**, 254001 (2021).
[18] N. B. Manson and J. P. Harrison, "Photo-ionization of the nitrogen-vacancy center in diamond," Diamond and Related Materials **14**, 1705–1710 (2005).

[19]S. Eldemrdash, G. Thalassinos, A. Alzahrani, Q. Sun, E. Walsh, E. Grant, H. Abe, T. L. Greaves, T. Ohshima, P. Cigler, P. Matějíček, D. A. Simpson, A. D. Greentree, G. Bryant, B. C. Gibson, and P. Reineck, "Fluorescent HPHT nanodiamonds have disk- and rod-like shapes," Carbon **206**, 268–276 (2023).

[20]C. Bradac, T. Gaebel, N. Naidoo, MJ. Sellars, J. Twamley, LJ. Brown, AS. Barnard, T. Plakhotnik, AV. Zvyagin, and JR. Rabeau, "Observation and control of blinking nitrogen-vacancy centres in discrete nanodiamonds," Nature nanotechnology **5**, 345 (2010).

[21]O. Shenderova, N. Nunn, T. Oeckinghaus, M. Torelli, G. McGuire, K. Smith, E. Danilov, R. Reuter, J. Wrachtrup, A. Shames, D. Filonova, and A. Kinev, "Commercial quantities of ultrasmall fluorescent nanodiamonds containing color centers," in *SPIE OPTO*, edited by Z. U. Hasan, P. R. Hemmer, H. Lee, and A. L. Migdall (San Francisco, California, United States, 2017) p. 1011803.

[22]K. Groot-Berning, N. Raatz, I. Dobrinets, M. Lesik, P. Spinicelli, A. Tallaire, J. Achard, V. Jacques, J.-F. Roch, A. M. Zaitsev, J. Meijer, and S. Pezzagna, "Passive charge state control of nitrogen-vacancy centres in diamond using phosphorous and boron doping," physica status solidi (a) **211**, 2268–2273 (2014).

[23]S. Dhomkar, H. Jayakumar, P. R. Zangara, and C. A. Meriles, "Charge Dynamics in near-Surface, Variable-Density Ensembles of Nitrogen-Vacancy Centers in Diamond," Nano Lett. **18**, 4046–4052 (2018).

[24]M. W. Doherty, V. M. Acosta, A. Jarmola, M. S. J. Barson, N. B. Manson, D. Budker, and L. C. L. Hollenberg, "Temperature shifts of the resonances of the NV^- center in diamond," Phys. Rev. B **90**, 041201 (2014).

[25]D. Aude Craik, P. Kehayias, A. Greenspon, X. Zhang, M. Turner, J. Schloss, E. Bauch, C. Hart, E. Hu, and R. Walsworth, "Microwave-Assisted Spectroscopy Technique for Studying Charge State in Nitrogen-Vacancy Ensembles in Diamond," Phys. Rev. Applied **14**, 014009 (2020).

[26]H.-Q. Zhao, M. Fujiwara, and S. Takeuchi, "Suppression of fluorescence phonon sideband from nitrogen vacancy centers in diamond nanocrystals by substrate effect," Opt. Express, OE **20**, 15628–15635 (2012).

[27]P. Reineck, L. F. Trindade, J. Havlik, J. Stursa, A. Heffernan, A. Elbourne, A. Orth, M. Capelli, P. Cigler, D. A. Simpson, and B. C. Gibson, "Not All Fluorescent Nanodiamonds Are Created Equal: A Comparative Study," Particle & Particle Systems Characterization **36**, 1900009 (2019).

[28]E. R. Wilson, L. M. Parker, A. Orth, N. Nunn, M. Torelli, O. Shenderova, B. C. Gibson, and P. Reineck, "The effect of particle size on nanodiamond fluorescence and colloidal properties in biological media," Nanotechnology **30**, 385704 (2019).

[29]D. J. McCloskey, N. Dontschuk, D. A. Broadway, A. Nadarajah, A. Stacey, J.-P. Tetienne, L. C. L. Hollenberg, S. Prawer, and D. A. Simpson, "Enhanced Widefield Quantum Sensing with Nitrogen-Vacancy Ensembles Using Diamond Nanopillar Arrays," ACS Appl. Mater. Interfaces **12**, 13421–13427 (2020).

[30]S. A. Savinov, V. V. Sychev, and D. Bi, "Diamond nitrogen-vacancy center charge state ratio determination at a given sample point," Journal of Luminescence **248**, 118981 (2022).

[31]A. Bhaumik, R. Sachan, and J. Narayan, "Tunable charge states of nitrogen-vacancy centers in diamond for ultrafast quantum devices," Carbon **142**, 662–672 (2019).

[32]F. Treussart, V. Jacques, E. Wu, T. Gacoin, P. Grangier, and J.-F. Roch, "Photoluminescence of single colour defects in 50 nm diamond nanocrystals," Physica B: Condensed Matter **376**, 926–929 (2006).

[33]S. Karaveli, O. Gaathon, A. Wolcott, R. Sakakibara, O. A. Shemesh, D. S. Peterka, E. S. Boyden, J. S. Owen, R. Yuste, and D. Englund, "Modulation of nitrogen vacancy charge state and fluorescence in nanodiamonds using electrochemical potential," PNAS **113**, 3938–3943 (2016).

[34]T.-I. Yang, Y.-W. Huang, P. Bista, C.-F. Ding, J. Chen, C.-T. Chiang, and H.-C. Chang, "Photoluminescence of Nitrogen-Vacancy Centers by Ultraviolet One- and Two-Photon Excitation of Fluorescent Nanodiamonds," J. Phys. Chem. Lett. , 11280–11287 (2022).

[35]K. Beha, A. Batalov, N. B. Manson, R. Bratschitsch, and A. Leitenstorfer, "Optimum Photoluminescence Excitation and Recharging Cycle of Single Nitrogen-Vacancy Centers in Ultrapure Diamond," Phys. Rev. Lett. **109**, 097404 (2012).

[36]M. Capelli, P. Reineck, D. W. M. Lau, A. Orth, J. Jeske, M. W. Doherty, T. Ohshima, A. D. Greentree, and B. C. Gibson, "Magnetic field-induced enhancement of the nitrogen-vacancy fluorescence quantum yield," Nanoscale **9**, 9299–9304 (2017).

[37]J.-P. Tetienne, L. Rondin, P. Spinicelli, M. Chipaux, T. Debuisschert, J.-F. Roch, and V. Jacques, "Magnetic-field-dependent photodynamics of single NV defects in diamond: An application to qualitative all-optical magnetic imaging," New J. Phys. **14**, 103033 (2012).

Supplementary information
Robust quantification of the diamond nitrogen-vacancy center charge state via photoluminescence spectroscopy

G. Thalassinos,[1] D. J. McCloskey,[2,3] A. Mameli,[1] A. J. Healey,[1] C. Pattinson,[2,3] D. Simpson,[2,3] B. C. Gibson,[1] A. Stacey,[1] N. Dontschuk,[2] and P. Reineck[1]

[1)] *School of Science, RMIT University, Melbourne, VIC 3001, Australia*

[2)] *School of Physics, University of Melbourne, Parkville, VIC 3010, Australia*

[3)] *Australian Research Council Centre of Excellence in Quantum Biotechnology, School of Physics, University of Melbourne, Parkville, VIC 3010, Australia*

I. NV EMISSION RANGES

Table S1 provides a summary of the approximate maximum emission wavelength of both NV^0 and NV^- observed across the literature. Data is organised as a function of diamond type and size, including excitation wavelength(s) (λ_{ex}) used in each study to investigate NV^0 and/or NV^-.

Generally, the maximum emission range of both NV charge states vary significantly throughout the literature, with no clear trend emerging as a function of diamond type or size. Works investigating NV fluorescence using blue (400–450 nm) excitation show negligible difference in maximum emission wavelengths between NV^0 and NV^-[4,10]. A similar observation can be made for works which derive "pure" NV spectra experimentally[7,11], which is contrasting against works using non-negative matrix factorization (NNMF), which suggests that NV^0 emits far less into the red spectrum compared to NV^-[6,13,15,16].

TABLE S1. Maximum emission wavelength as measured/predicted by different studies. Boldface denotes NV^0/NV^- spectral profiles derived using NNMF.

Author(s)	Diamond type/size	λ_{ex} [nm]	Max. emission wavelength [nm]		Ref.
			NV^0	NV^-	
Gruber et al.	Type Ib	514	—	900	1
Jeske et al.	Type Ib	53	830	870	2
Kurtsiefer et al.	Type Ib	532	—	760	3
Manson et al.	Type Ib	445 (NV^0), 532 (NV^-)	850	850	4
Manson and Harrison	Type Ib	532	>740	>740	5
Savinov et al.	**Type Ib**	**532**	**740**	**>800**	6
Alsid et al.	Type IIa	532	>800	>800	7
Beha et al.	Type IIa	521, 550	—	<800	8
Groot-Berning et al.	Type IIa	532	850	850	9
Aslam et al.	Type IIa	440 (NV^0), 514 (NV^-)	850	850	10
Aude Craik et al.	Type IIa	532	850	850	11
Dhomkar et al.	Type IIa	532	—	800	12
McCloskey et al.	**Type IIa**	**532**	**775**	**850**	13
Bhaumik et al.	—	532	>750	>750	14
Reineck et al.	**HPHT ND, 100–200 nm**	**520**	**720**	**790**	15
Wilson et al.	**HPHT ND, 10–140 nm**	**510**	**725**	**850**	16
Mohtashami and Koenderink	HPHT ND, 26–108 nm	532	—	850	17
Rondin et al.	HPHT ND, 10–100 nm	532	<800	<800	18
Treussart et al.	HPHT ND, 50 nm	514.5	<800	<800	19
Faklaris et al.	HPHT ND, <50 nm	532	—	<800	20
Faklaris et al.	HPHT ND, <50 nm	488	720	—	21
Berthel et al.	HPHT ND, 25 nm	515	—	>800	22
Karaveli et al.	HPHT ND, <20 nm	532	800	800	23
Bradac et al.	DND, 5 nm	532	—	840	24

II. SAMPLES

Table S2 provides a summary of samples used throughout this work and which figures they appear in.

TABLE S2. Summary of investigated samples.

Sample	System	Shown in figure(s)	Manufacturer
Bulk DNV-B14	Confocal	1A, 3A-B, 5A-F, S2-S7	Element Six
140 nm HPHT FND	Solution	2A-C	Adàmas Nano.
100 nm HPHT FND	Confocal	3E-F, S9	Adàmas Nano.
20 nm HPHT FND	Solution	3C-D, S8	Adàmas Nano.

III. OPTICAL SETUPS

Schematics of our custom-built scanning confocal microscope and in-solution spectroscopy setup can be seen in fig. S1.

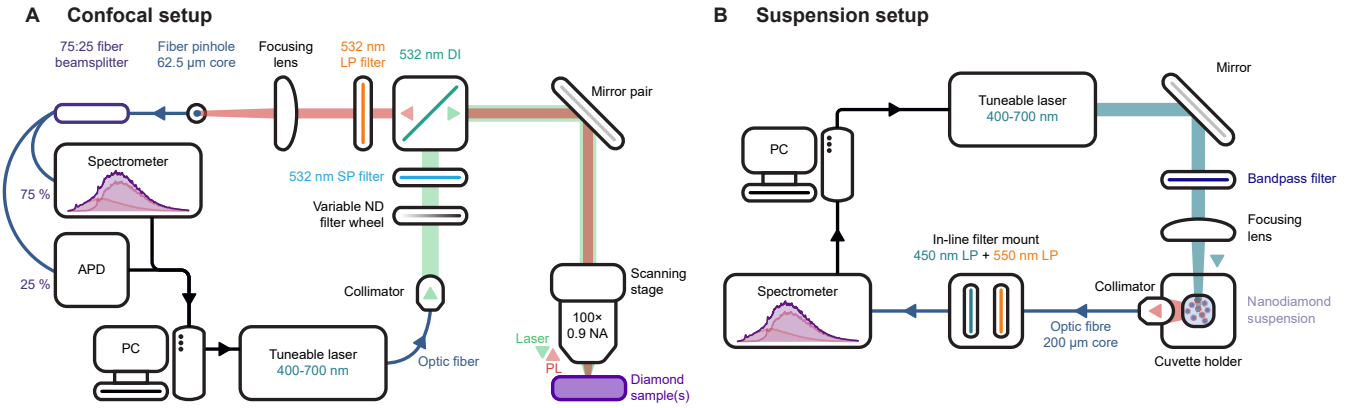


FIG. S1. Schematics of custom built confocal (A) and suspension (B) setups. **A:** A fibre coupled, pulsed tuneable laser is sent through a 532 nm SP filter and variable ND filter to control excitation power and guided to the sample through a 532 nm DI mirror and a pair of mirrors. An XYZ scanning stage with a 100× objective (NA = 0.9) probes the diamond sample(s). Fluorescence is collected through the objective and is focused onto a multi-mode fibre with a in-built beamsplitter, which sends 75 % of the signal to the spectrometer and the remaining 25 % to an APD. **B:** A tuneable laser is reflected off a mirror, through a bandpass filter and focused onto a cuvette holding the nanodiamond suspension. Fluorescence is collected through a multi-mode fibre, sent through an in-line filter mount, then coupled to a spectrometer.

IV. NV CHARGE STATE DETERMINATION PROTOCOLS

A. Dual excitation protocol

Here, we show individual fits using each of the NV charge state ratio determination techniques used to produce the data in figure 3B of the main text. Figure S2 shows our dual excitation protocol (DEP) on bulk diamond across excitation wavelengths between 405–520 nm, with reference NV^0/NV^- spectra shown in Figure S2A.

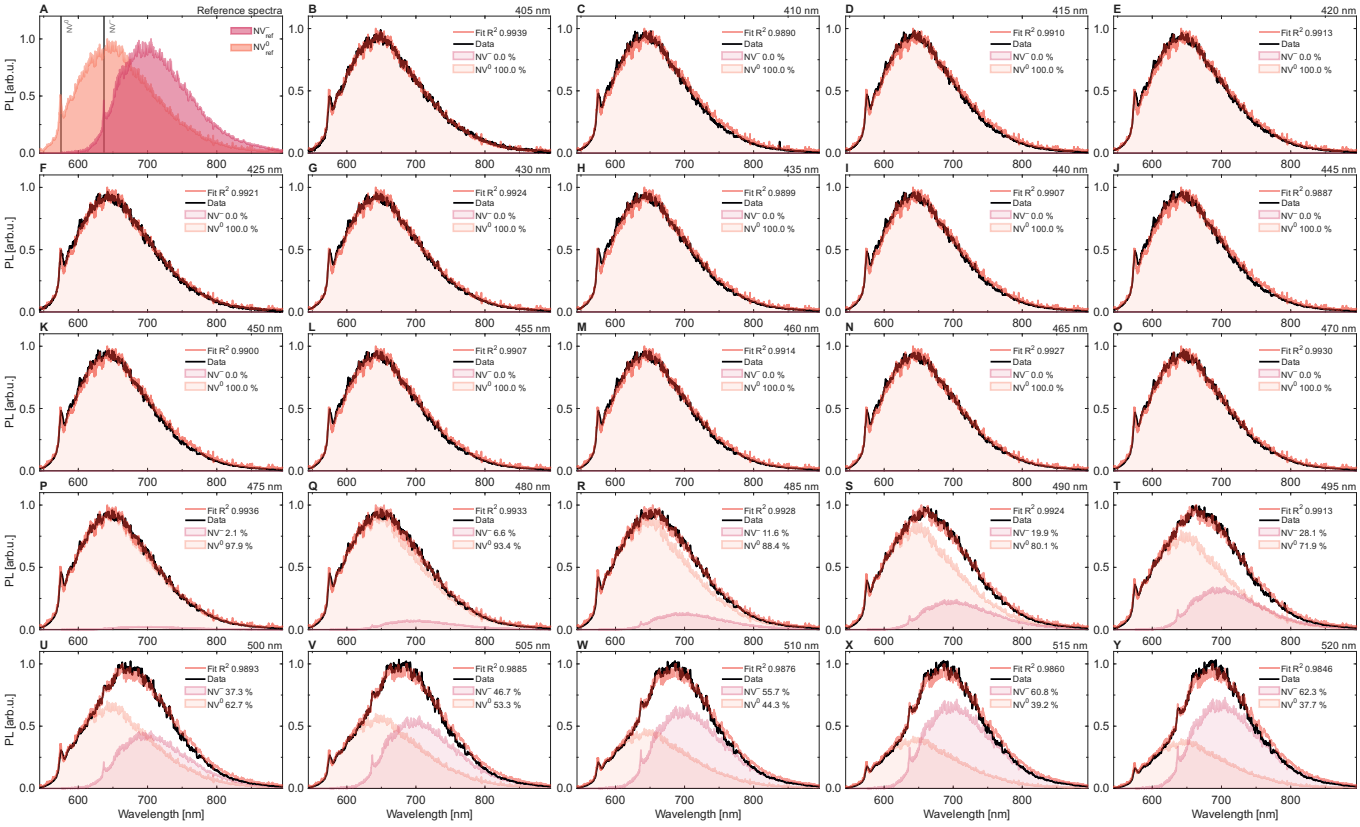


FIG. S2. NV charge state analysis via dual excitation protocol (DEP) on DNV-B14. **A:** Predicted pure NV^0 and NV^- spectra based on DEP. **B-Y:** Fitting of DEP NV spectra to fluorescence spectra taken for excitation wavelengths between 405–520 nm in increments of 5 nm and a laser bandwidth of 10 nm.

B. Skewed Gaussian fitting

For skewed Gaussian (SG) fitting, we used a custom fit equation to approximate the NV fluorescence spectra. We used a combination of two regular Gaussian functions to model both NV^0 and NV^- zero-phonon lines (ZPLs) and two skewed Gaussians for their respective phonon side-bands (PSBs) via

$$\begin{aligned} S_{\mathrm{NV}}(\lambda) = A_{\mathrm{ZPL1}} \cdot \exp\left(-\frac{(\lambda-\lambda_{\mathrm{ZPL1}})^2}{2\nu_{\mathrm{ZPL1}}^2}\right) + A_{\mathrm{PSB1}} \cdot \exp\left(-\left(\frac{\lambda-\lambda_{\mathrm{PSB1}}}{\nu_{\mathrm{PSB1}}}\right)^2\right) \cdot \left(1+\mathrm{erf}\left(\alpha_1 \cdot \frac{\lambda-\lambda_{\mathrm{PSB1}}}{\nu_{\mathrm{PSB1}}}\right)\right) + \\ A_{\mathrm{ZPL2}} \cdot \exp\left(-\frac{(\lambda-\lambda_{\mathrm{ZPL2}})^2}{2\nu_{\mathrm{ZPL2}}^2}\right) + A_{\mathrm{PSB2}} \cdot \exp\left(-\left(\frac{\lambda-\lambda_{\mathrm{PSB2}}}{\nu_{\mathrm{PSB2}}}\right)^2\right) \cdot \left(1+\mathrm{erf}\left(\alpha_2 \cdot \frac{\lambda-\lambda_{\mathrm{PSB2}}}{\nu_{\mathrm{PSB2}}}\right)\right), \end{aligned} \tag{1}$$

where erf is the error function, given by

$$\mathrm{erf}(x) = \frac{2}{\sqrt{\pi}} \int_0^x e^{-t^2} dt. \tag{2}$$

We restricted all free parameters to a small window of acceptable values, enough to fit all combinations of NV^0 and NV^-. However, we could not find a set of parameters that would allow one pair of NV^0/NV^- reference spectra to fit the full series of data. Thus, the reference NV^0/NV^- spectra were slightly different for each excitation wavelength. These differences can be seen in fig. S3A, where all NV^0 and NV^- reference spectra are presented together. Despite these differences, we were able to fit all experimental data (fig. S3B–Y) using this technique and measure a systematic change in the NV charge state ratio.

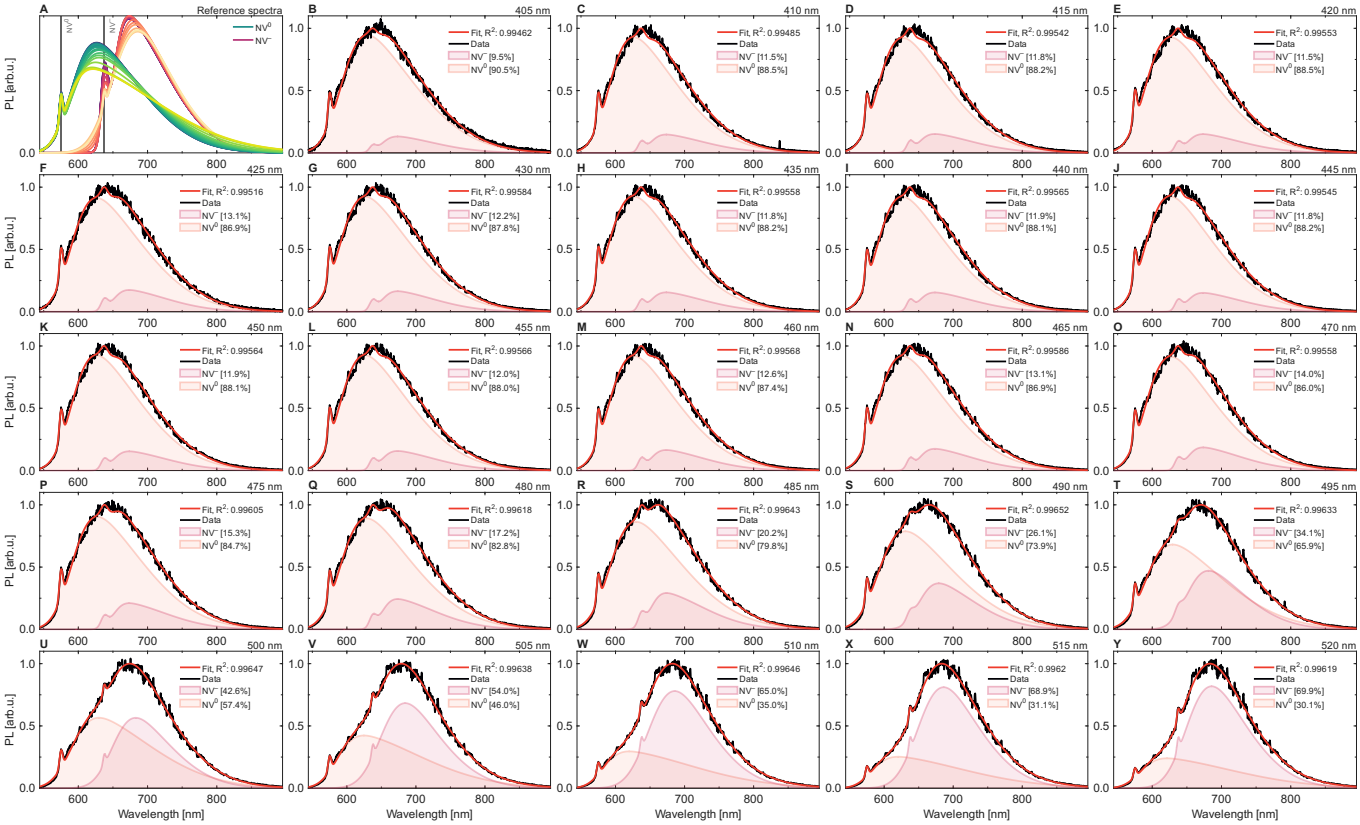


FIG. S3. NV charge state analysis via skewed Guassian (SG) fitting on DNV-B14. **A:** Reference NV^0/NV^- spectra used to fit experimental data. Fit parameters differed slightly for each measurement, leading to different NV reference spectra. **B-Y:** Fitting of DEP NV spectra to fluorescence spectra taken for excitation wavelengths between 405–520 nm in increments of 5 nm and a laser bandwidth of 10 nm.

C. Non-negative matrix factorization

For non-negative matrix factorization (NNMF), we used all background-corrected data for excitation wavelengths 405–520 nm as inputs for the 'nnmf' function in MATLAB, assuming 2 components. The outputs are shown in fig. S4A, with fits for each measurement across fig. S4B–Y.

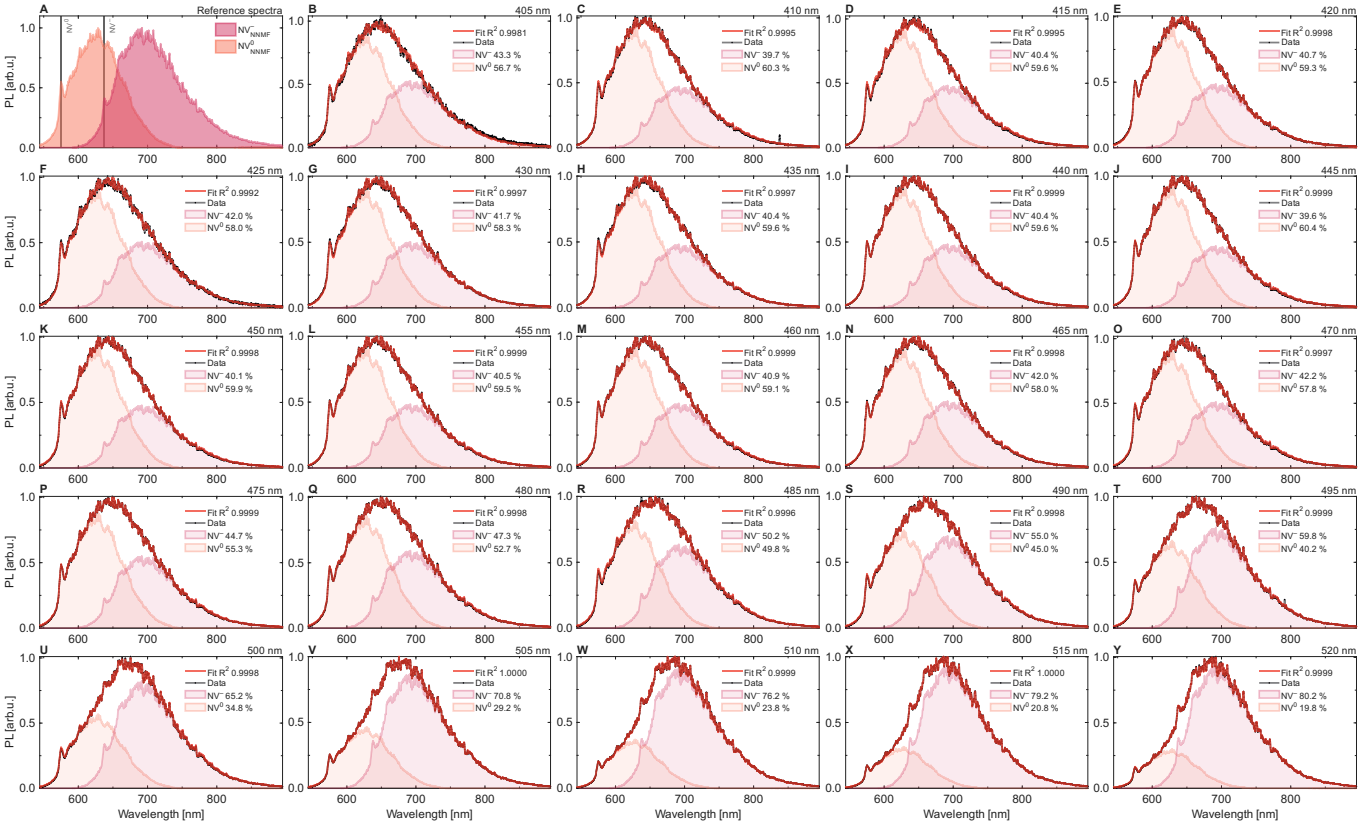


FIG. S4. NV charge state analysis via NNMF on DNV-B14. **A:** Predicted pure NV^0 and NV^- spectra based on NNMF. **B-Y:** Fitting of NNMF NV spectra to fluorescence spectra taken for excitation wavelengths between 405–520 nm in increments of 5 nm and a laser bandwidth of 10 nm.

D. Zero-phonon line fitting

Finally, for our ZPL method, we started by fitting two second order polynomials around both NV ZPLs at 575 and 637 nm, ignoring counts ±5 nm around each ZPL. This baseline, which represented fluorescence originating from the PSBs, rather than the ZPLs, was set to 0. We then fit a Gaussian (or Lorentzian, sample-dependent) function onto each ZPL and integrated the area under the curve to calculate the NV^0/NV^- ZPL intensities (I_{NV}). The NV^- contribution is then given as

$$NV^-[\%] = \frac{I_{NV^-}}{I_{NV^0} + I_{NV^-}}. \tag{3}$$

Figure S5 shows ZPL fitting for each excitation wavelength for the bulk sample. The relative contribution of each charge state is shown as part of the legend in each panel (A–X) with values in parentheses denoting uncertainty originating from uncertainties in each fit.

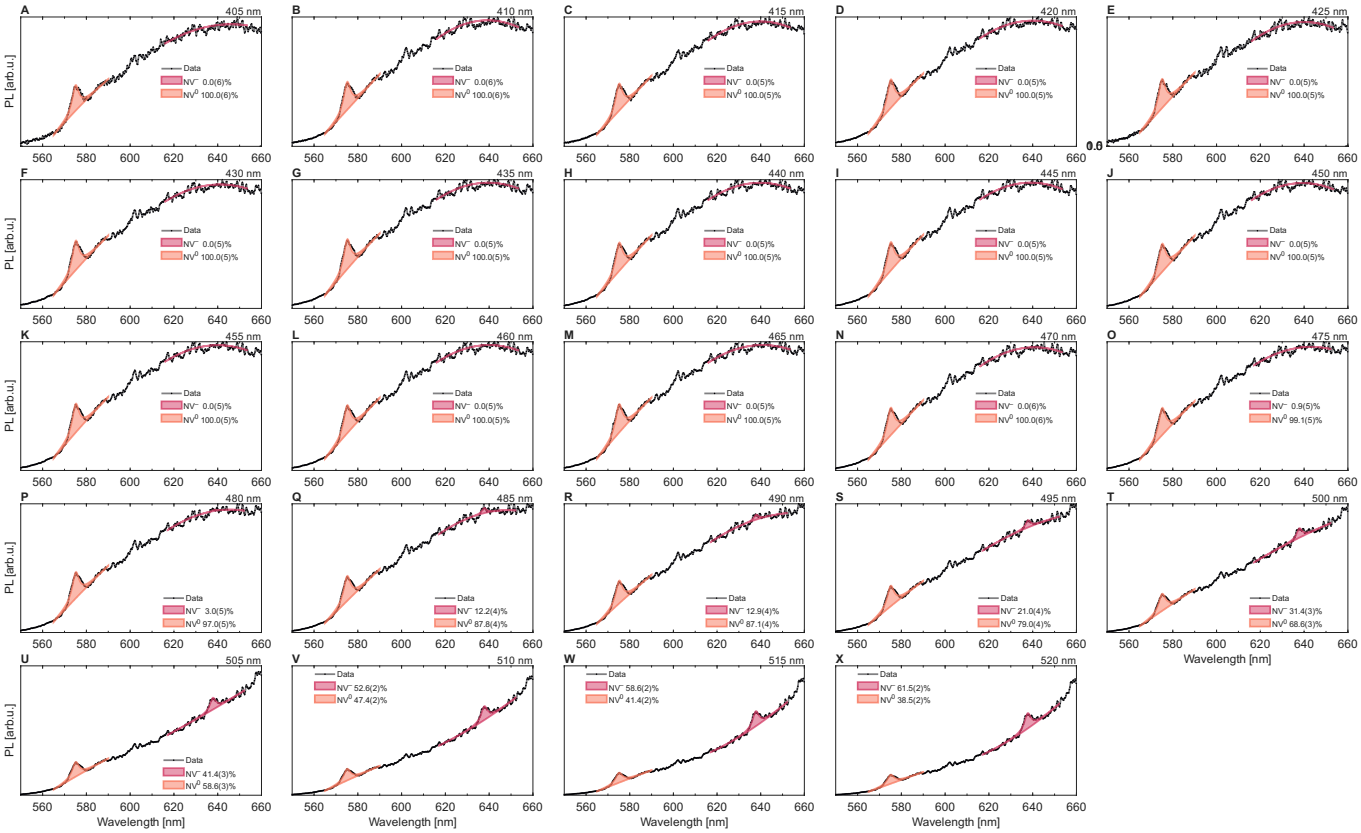


FIG. S5. NV charge state analysis via ZPL fitting on DNV-B14. **A-X:** Fitting of NV^0/NV^- ZPL for spectra taken under excitation wavelengths between 405–520 nm in increments of 5 nm and a laser bandwidth of 10 nm.

E. Technique validity

For DEP, SG, and NNMF, we calculated the R^2 values of each individual measurement shown in figs. S2 to S4 to quantify how well each method models the NV fluorescence spectra for different NV charge state ratios, shown in fig. S6. All three techniques show high R^2 values across the NV charge state ratio range we observed, with minimum R^2 value of 0.9846, and NNMF demonstrating the best fitting across the full range of excitation wavelengths. However, while both NNMF and SG models fit the experimental data better than our DEP, neither model can be physically justified.

We show in fig. S3A that the only way to achieve a good fit using our SG model is to allow fitting parameters to change per measurement. This leads to significantly different reference NV^0/NV^- spectra depending on the NV charge state ratio. However, we know that the fluorescence spectral profiles of both NV^0 and NV^- are fixed quantities for a given sample. Therefore, the NV charge state ratio calculated using this technique is unlikely to represent the "true" NV charge state ratio.

In the case of NNMF, which shows the best overall fitting with an average R^2 value of 0.9997, we see that the prediction for pure NV^0 shows emission only up to ≈750 nm (fig. S4A), significantly shorter than experimental evidence across the literature (see table S1) and predictions made by other techniques[7,11].

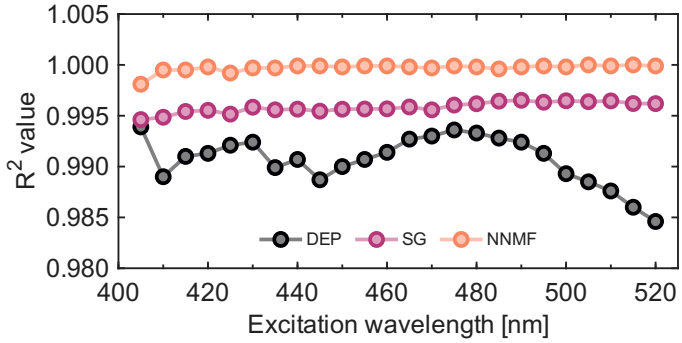


FIG. S6. R^2 values of all fits corresponding to figures S1–3.

We show a direct comparison between the NV^0/NV^- reference spectra derived from each of the three techniques in fig. S7. While each approach predicts similar a NV^- spectrum, with NNMF and DEP being indistinguishable, the NV^0 spectral profiles between the three methods vary significantly, highlighting the fundamental challenge: that NV^0 is difficult to verify.

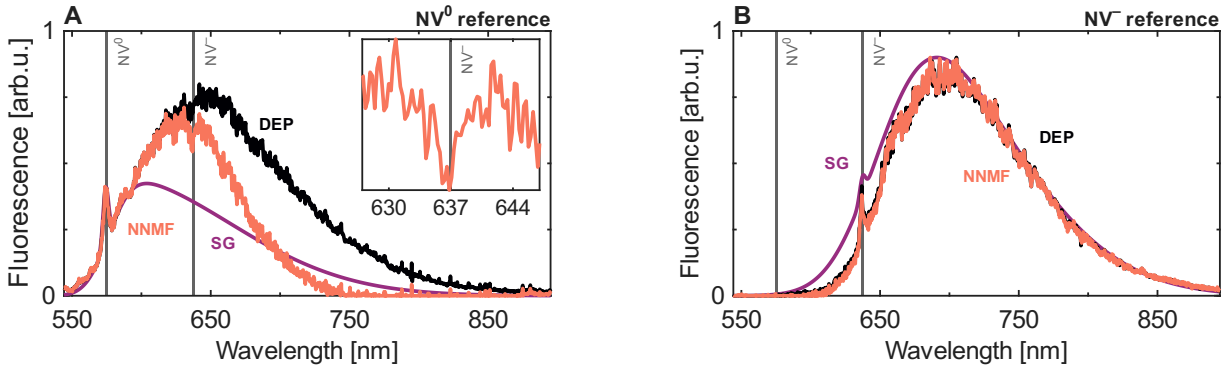


FIG. S7. NV^0/NV^- spectral profiles of bulk diamond as derived via DEP, NNMF, and SG fitting used to fit spectra in figs. S2 to S4, for figure 3 of the main text. **A:** NV^0 spectral profiles normalized to 575 nm showing significant variation at wavelengths >600 nm. The inset shows how the NNMF estimate of NV^0 has a dip at the NV^- ZPL, indicating that it may be underestimating NV^0. **B:** NV^- spectral profile which shows DEP and NNMF deriving identical results, while SG fitting results in a close-approximation to NV^-. Dashed lines represent the locations of the NV ZPLs.

V. CONFOCAL FLUORESCENCE MAP OF FLUORESCENT NANODIAMONDS

Figure S8 shows a confocal fluorescence map of the 100 nm FND particles investigated for figure 3E-F of the main text. The fluorescence map was taken under 520 nm excitation with a 550 nm long pass collection filter using our scanning confocal microscope (fig. S1A). The white circles identify particles which were analyzed with our spectrometer.

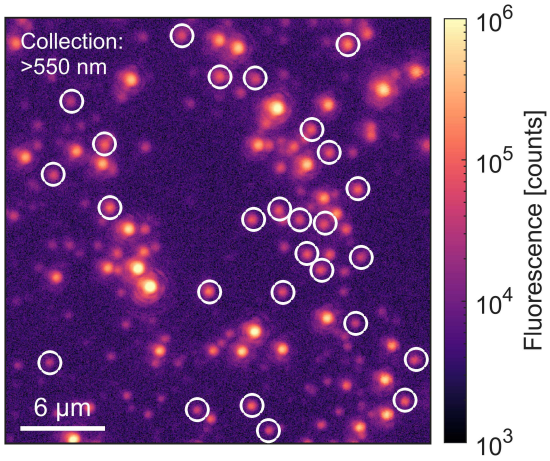


FIG. S8. Confocal fluorescence map of 100 nm FND particles spin coated onto a Si wafer substrate excited with 520 nm and and collected through a 550 nm long pass filter. White circles mark particles which were analyzed.

VI. BACKGROUND CORRECTIONS FOR IN-SOLUTION MEASUREMENTS

Nanoparticles in suspension represent one of the more challenging environments for determining the NV charge state ratio due to the overlap of multiple background signals. Under optimal NV excitation conditions of 510–540 nm, the peak of the water Raman spectrum overlaps significantly with NV fluorescence at 617–661 nm. Furthermore, nanodiamond particles of different sizes and concentrations have different scattering properties, leading to differences in the total intensity of the measured water Raman signal, which is further convoluted by variations in particle brightness. Therefore, it is non-trivial to determine how much the water Raman signal contributes to the overall measured signal compared to a pure water reference measurement. Under these conditions, there is no available experimental NV reference spectrum which can be used to accurately remove the background signals from the measured spectrum.

To precisely remove all background signals and isolate NV fluorescence, we use a combination of multiple background references and skewed Gaussian (SG) fitting. In fig. S3, we show that our SG model (eq. (1)) can be used to fit NV^0/NV^- spectra. Therefore, we can use this NV fluorescence spectrum model ($S_{NV}(\lambda)$) with additional parameters representing the scaling of the background references to fit the raw data (S_T) via

$$S_T(\lambda) = S_{NV}(\lambda) + \kappa_1 S_1(\lambda) + \kappa_2 S_2(\lambda) ... + \kappa_n S_n, \tag{4}$$

where S_n and κ_n represent the n^{th} reference spectrum and it's non-negative scaling, respectively. For nanodiamonds in DI water, we recorded the spectrometer dark counts ($S_{DC}(\lambda)$), a pure water reference ($S_{H_2O}(\lambda)$), and non-fluorescent SiO_2 nanoparticles (nominal size 40 nm) suspended in water ($S_{SiO_2}(\lambda)$) as our background signals. A thorough demonstration of our background removal steps is illustrated in fig. S9.

Here, we show each of the measurements (nanodiamonds, dark counts, water, and SiO_2 particles) as they were recorded (fig. S9A-C) and with overlapping signals removed (fig. S9D-F). For both nanodiamonds and the water Raman reference, we simply subtracted the dark counts. However, with the SiO_2 particles, we had to also remove the water Raman signal to isolate the scattering reference. We then fit the nanodiamond data using eq. (4), with each individual component of the model shown separately as shaded areas, as illustrated in fig. S9G. We demonstrate that this model fits the nanodiamond data with a high degree of confidence ($R^2 = 0.999$), allowing us to further identify outliers in the signal arising from cosmic rays interacting with our spectrometer. We can then remove all background signals, isolating NV fluorescence (fig. S9H).

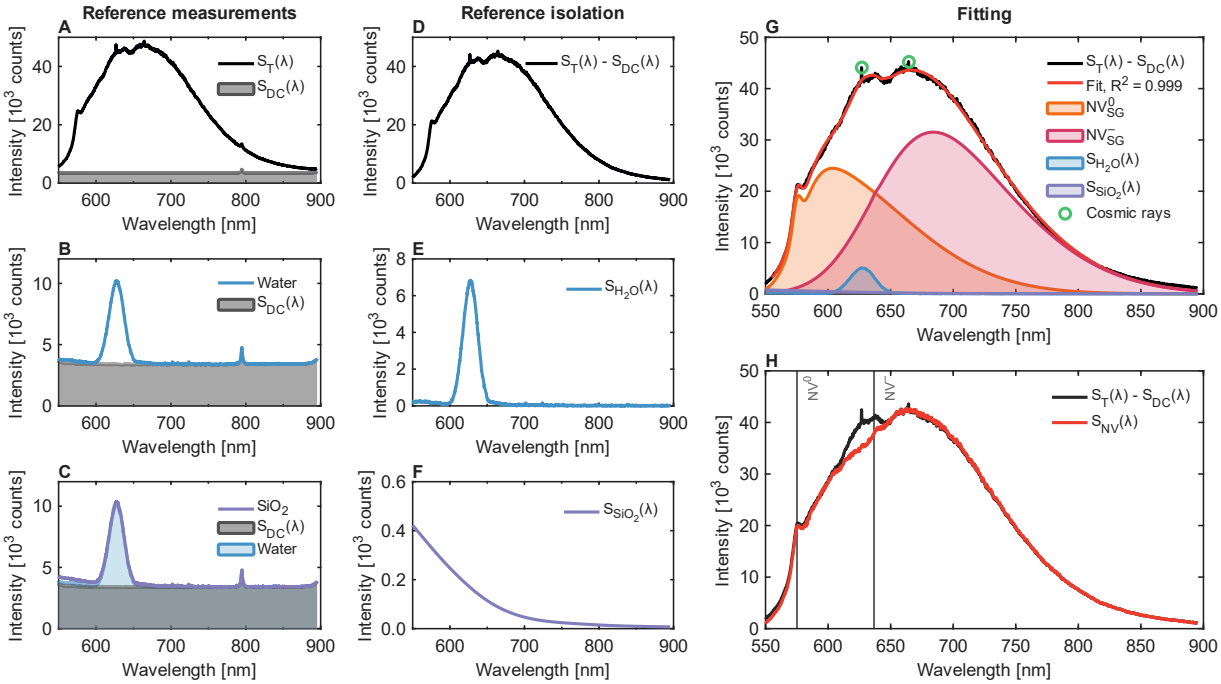


FIG. S9. Background correction for in-solution measurements. **A:** Raw data of nanodiamond fluorescence measured in DI water suspension ($S_T(\lambda)$) and spectrometer dark counts ($S_{\mathrm{DC}}(\lambda)$). **B:** Raw nanodiamond data with dark counts removed. **C:** Water Raman reference measurement with dark counts. **D:** Pure water reference spectrum under 520 nm excitation. **E:** Measurement of 40 nm SiO_2 nanoparticles suspended in DI water. **F:** Scattering reference with dark counts and water Raman signals removed. **G:** Fitting of nanodiamond signal using NV SG model ($NV^0{}_{\mathrm{SG}}/NV^-{}_{\mathrm{SG}}$), water, and scattering references, with cosmic rays identified by marked circles. **H:** Comparison before and after the removal of water Raman, scattering, and cosmic ray signals from the nanodiamond sample, showing isolation of NV fluorescence.

REFERENCES

[1] A. Gruber, A. Dräbenstedt, C. Tietz, L. Fleury, J. Wrachtrup, and C. Von Borczyskowski, "Scanning confocal optical microscopy and magnetic resonance on single defect centers," Science **276**, 2012–2014 (1997).

[2] J. Jeske, D. W. M. Lau, X. Vidal, L. P. McGuinness, P. Reineck, B. C. Johnson, M. W. Doherty, J. C. McCallum, S. Onoda, F. Jelezko, T. Ohshima, T. Volz, J. H. Cole, B. C. Gibson, and A. D. Greentree, "Stimulated emission from nitrogen-vacancy centres in diamond," Nat Commun **8**, 14000 (2017).

[3] C. Kurtsiefer, S. Mayer, P. Zarda, and H. Weinfurter, "Stable solid-state source of single photons," Physical review letters **85**, 290 (2000).

[4] N. B. Manson, M. Hedges, M. S. J. Barson, R. Ahlefeldt, M. W. Doherty, H. Abe, T. Ohshima, and M. J. Sellars, "NV^-–N^+ Pair Centre in 1b Diamond," New J. Phys. **20**, 113037 (2018).

[5] N. B. Manson and J. P. Harrison, "Photo-ionization of the nitrogen-vacancy center in diamond," Diamond and Related Materials **14**, 1705–1710 (2005).

[6] S. A. Savinov, V. V. Sychev, and D. Bi, "Diamond nitrogen-vacancy center charge state ratio determination at a given sample point," Journal of Luminescence **248**, 118981 (2022).

[7] S. T. Alsid, J. F. Barry, L. M. Pham, J. M. Schloss, M. F. O'Keeffe, P. Cappellaro, and D. A. Braje, "Photoluminescence Decomposition Analysis: A Technique to Characterize N-V Creation in Diamond," Phys. Rev. Applied **12**, 044003 (2019).

[8] K. Beha, A. Batalov, N. B. Manson, R. Bratschitsch, and A. Leitenstorfer, "Optimum Photoluminescence Excitation and Recharging Cycle of Single Nitrogen-Vacancy Centers in Ultrapure Diamond," Phys. Rev. Lett. **109**, 097404 (2012).

[9] K. Groot-Berning, N. Raatz, I. Dobrinets, M. Lesik, P. Spinicelli, A. Tallaire, J. Achard, V. Jacques, J.-F. Roch, A. M. Zaitsev, J. Meijer, and S. Pezzagna, "Passive charge state control of nitrogen-vacancy centres in diamond using phosphorous and boron doping," physica status solidi (a) **211**, 2268–2273 (2014).

[10] N. Aslam, G. Waldherr, P. Neumann, F. Jelezko, and J. Wrachtrup, "Photo-induced ionization dynamics of the nitrogen vacancy defect in diamond investigated by single-shot charge state detection," New J. Phys. **15**, 013064 (2013).

[11] D. Aude Craik, P. Kehayias, A. Greenspon, X. Zhang, M. Turner, J. Schloss, E. Bauch, C. Hart, E. Hu, and R. Walsworth, "Microwave-Assisted Spectroscopy Technique for Studying Charge State in Nitrogen-Vacancy Ensembles in Diamond," Phys. Rev. Applied **14**, 014009 (2020).

[12] S. Dhomkar, H. Jayakumar, P. R. Zangara, and C. A. Meriles, "Charge Dynamics in near-Surface, Variable-Density Ensembles of Nitrogen-Vacancy Centers in Diamond," Nano Lett. **18**, 4046–4052 (2018).

[13] D. J. McCloskey, N. Dontschuk, D. A. Broadway, A. Nadarajah, A. Stacey, J.-P. Tetienne, L. C. L. Hollenberg, S. Prawer, and D. A.

Simpson, "Enhanced Widefield Quantum Sensing with Nitrogen-Vacancy Ensembles Using Diamond Nanopillar Arrays," ACS Appl. Mater. Interfaces **12**, 13421–13427 (2020).
[14]A. Bhaumik, R. Sachan, and J. Narayan, "Tunable charge states of nitrogen-vacancy centers in diamond for ultrafast quantum devices," Carbon **142**, 662–672 (2019).
[15]P. Reineck, L. F. Trindade, J. Havlik, J. Stursa, A. Heffernan, A. Elbourne, A. Orth, M. Capelli, P. Cigler, D. A. Simpson, and B. C. Gibson, "Not All Fluorescent Nanodiamonds Are Created Equal: A Comparative Study," Particle & Particle Systems Characterization **36**, 1900009 (2019).
[16]E. R. Wilson, L. M. Parker, A. Orth, N. Nunn, M. Torelli, O. Shenderova, B. C. Gibson, and P. Reineck, "The effect of particle size on nanodiamond fluorescence and colloidal properties in biological media," Nanotechnology **30**, 385704 (2019).
[17]A. Mohtashami and A. F. Koenderink, "Suitability of nanodiamond nitrogen–vacancy centers for spontaneous emission control experiments," New J. Phys. **15**, 043017 (2013).
[18]L. Rondin, G. Dantelle, A. Slablab, F. Grosshans, F. Treussart, P. Bergonzo, S. Perruchas, T. Gacoin, M. Chaigneau, H.-C. Chang, V. Jacques, and J.-F. Roch, "Surface-induced charge state conversion of nitrogen-vacancy defects in nanodiamonds," Phys. Rev. B **82**, 115449 (2010).
[19]F. Treussart, V. Jacques, E. Wu, T. Gacoin, P. Grangier, and J.-F. Roch, "Photoluminescence of single colour defects in 50 nm diamond nanocrystals," Physica B: Condensed Matter **376**, 926–929 (2006).
[20]O. Faklaris, J. Botsoa, T. Sauvage, J.-F. Roch, and F. Treussart, "Photoluminescent nanodiamonds: Comparison of the photoluminescence saturation properties of the NV color center and a cyanine dye at the single emitter level, and study of the color center concentration under different preparation conditions," Diamond and Related Materials Proceedings of Diamond 2009, The 20th European Conference on Diamond, Diamond-Like Materials, Carbon Nanotubes and Nitrides, Part 2, **19**, 988–995 (2010).
[21]O. Faklaris, V. Joshi, T. Irinopoulou, P. Tauc, M. Sennour, H. Girard, C. Gesset, J.-C. Arnault, A. Thorel, J.-P. Boudou, *et al.*, "Photoluminescent diamond nanoparticles for cell labeling: Study of the uptake mechanism in mammalian cells," ACS nano **3**, 3955–3962 (2009).
[22]M. Berthel, O. Mollet, G. Dantelle, T. Gacoin, S. Huant, and A. Drezet, "Photophysics of single nitrogen-vacancy centers in diamond nanocrystals," Phys. Rev. B **91**, 035308 (2015).
[23]S. Karaveli, O. Gaathon, A. Wolcott, R. Sakakibara, O. A. Shemesh, D. S. Peterka, E. S. Boyden, J. S. Owen, R. Yuste, and D. Englund, "Modulation of nitrogen vacancy charge state and fluorescence in nanodiamonds using electrochemical potential," PNAS **113**, 3938–3943 (2016).
[24]C. Bradac, T. Gaebel, N. Naidoo, MJ. Sellars, J. Twamley, LJ. Brown, AS. Barnard, T. Plakhotnik, AV. Zvyagin, and JR. Rabeau, "Observation and control of blinking nitrogen-vacancy centres in discrete nanodiamonds," Nature nanotechnology **5**, 345 (2010).